Journal of Materials Chemistry C

Accepted Manuscript

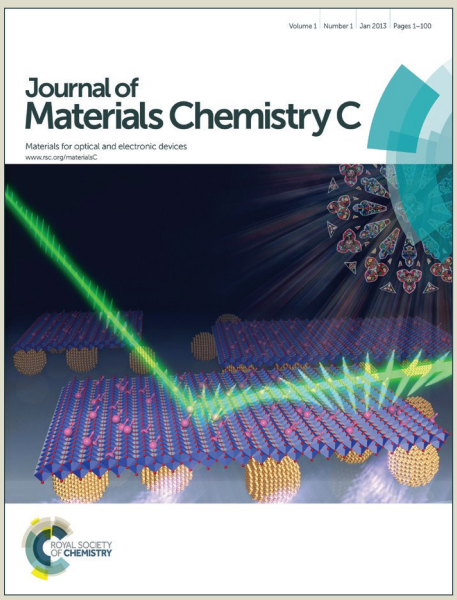

ROYAL SOCIETY OF CHEMISTRY

www.rsc.org/materialsC

Electronic Properties of Two-Dimensional Van der Waals GaS/GaSe Heterostructures

Wei Wei,[1] Ying Dai,[*,1] Chengwang Niu,[2] Xiao Li,[3] Yandong Ma,[4] and Baibiao Huang[1]

[1]School of Physics, State Key Laboratory of Crystal Materials, Shandong University, Jinan 250100, China

[2]Peter Grünberg Institut and Institute for Advanced Simulation, Forschungszentrum Jülich and JARA, 52425 Jülich, Germany

[3]Department of Physics, University of Texas at Austin, Austin, Texas 78712, United States

[4]Department of Physics and Earth Science, Jacobs University Bremen, Campus Ring 1, 28759 Bremen, Germany

Corresponding Author: Ying Dai (Y.D.)

daiy60@sdu.edu.cn

Abstract

On the basis of density functional electronic calculations, heterostructures of single-layer GaS and GaSe were found to exhibit novel physical properties due to the specific interfacing effects and versatile structural features. We verified that electrons and holes can be distributed on the opposite constituent of the heterostructures, forming a type-II band alignment and enabling physical separation of excitons, which is highly desirable in applications in such as solar energy conversion. We found the Rashba effects in the two-dimensional GaS/GaSe heterostructures due to the breaking of inversion symmetry and the intrinsic polarization, which reveals new possibility in applications in spintronic and electronic nanodevices. In addition, we confirmed that the electronic properties of GaS/GaSe van der Waals heterostructures can be continuously tuned by external strain.

A table of contents

The exciton separation and Rashba spin splitting have been demonstrated in the van der Waals GaS/GaSe heterostructures.

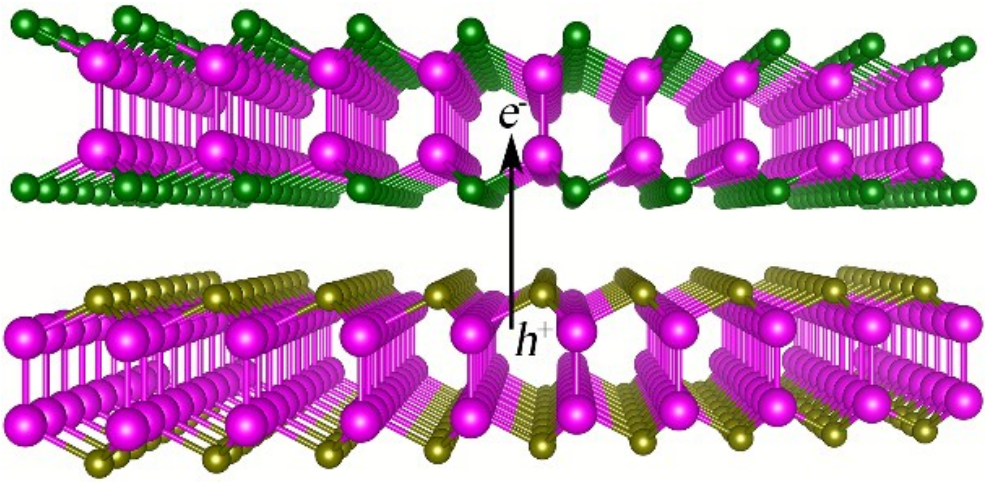

1. Introduction

Group-III monochalcogenides (GaX with X=S and Se) have been attracting intense attention due to their exotic physical and chemical properties,[1-6] with great promise for applications in fields such as solar energy conversion and optoelectronics.[7-12] In bulk phase, layered GaX is constructed by four-atom planes covalently bonded in sequence of X-Ga-Ga-X with a D_{3h} symmetry, while the interlayer coupling is dominated by weak van der Waals forces. On the basis of first-principles density functional theory (DFT) calculations, the formation energies of GaX are identified to be comparable to that of single-layer MoS_2 implying that it is easily to mechanically extract single-layer GaS and GaSe from their layered bulk counterparts.[13] In searching for other two-dimensional materials beyond graphene, the successful access of single-layer GaS and GaSe marks the expansion of two-dimensional materials' family and opens up new possibilities in applications in such as field-effect transistors.[7,8] In recent experiments, photoresponse behaviors of single-layer GaS and GaSe were demonstrated and they were identified to be promising candidates for photodetector due to the strong absorption in ultraviolet-visible wavelength region.[9-12] As reported in previous experiments, single-layer GaSe exhibits light responsivity (at 254 nm) orders of magnitude higher than the similar devices made from graphene, MoS_2 or other two-dimensional materials-based devices.[9,10] In addition, single-layer GaS and GaSe express high potential as photocatalyst for water splitting due to the suitable band edge positions with respect to the redox potentials of water.[13] As we know, in the processes of photodetecting and photocatalysis, efficient separation of photoinduced electron-

hole pairs plays a crucial role in determining the efficiency.

Interface between semiconductors becomes the central concept in modern materials science and technology, opening up possibilities to create new material systems with novel physical effects and rich functionalities.[14,15] At present, interfaces have been realized in two-dimensional materials. In heterostructures of MoS_2 and WS_2, for example, a strong interlayer excitonic transition was observed,[16] and the interlayer interaction and optical properties could be externally tuned.[17,18] In the case of graphene/MoS_2 heterobilayers, addition of graphene increases the electron conductivity of MoS_2 and, as a consequence, graphene/MoS_2 heterostructures hold yet untapped promise for application as solar cells with the conversion efficiency of up to 1%.[19,20] In this sense, heterostructures between two-dimensional materials could be basic building blocks with distinct physical and optical properties for a wide range of applications. Inspired by the advancements in experiments, we studied the interfacing effects between single-layer GaS and GaSe. It is of interest and importance that two-dimensional GaS/GaSe heterostructures reveal new insights into the physical and chemical properties.

2. Methodology

The first-principles DFT calculations were performed using the projector augmented wave (PAW) scheme, as implemented in the plane-wave basis code VASP (Vienna *ab initio* simulation package).[21,22] The generalized gradient approximation (GGA)[23] as formulated by Perdew-Burke-Ernzerhof (PBE)[24] was introduced for the exchange and

correlation contributions. A cutoff energy of 470 eV was chosen for the plane-wave expansion of wave functions and the self-consistent convergence accuracy was set at 10^{-4} eV/atom. The Monkhorst-Pack scheme of ***k***-point sampling was adopted for the integration over the first Brillouin zone.[25] A 23×23 surface grid was used to relax the single-layer GaS and GaSe, and a slab model with vacuum spacing of larger than 30 Å was adopted to eliminate the spurious interactions between periodic imagines. In cases of calculating the GaS/GaSe heterostructures, the ***k***-point grid of 19×19 and the vacuum spacing of larger than 27 Å were used. We confirmed that the ***k***-point grid and vacuum spacing are sufficient to obtain the converged results. In structural relaxation, residual Hellmann-Feynman forces were set to 0.02 eV/Å within the conjugate gradient algorithm. The Gaussian smearing was used to address how the partial occupancies are set for each wave function and the width of smearing was 0.1 eV. In order to take the van der Walls forces into account to better describe the nonbonding interactions, a semi-empirical dispersion potential was added to the conventional Kohn-Sham DFT energy in scheme of DFT-D2 method[26] for calculations of the GaS/GaSe heterostructures. The spin-orbital coupling (SOC) effects were treated self-consistently in fully relativistic pseudopotentials for valence electrons.[27]

3. Results and discussion

In bulk phases of GaS and GaSe, the weak van der Waals interlayer interaction allows different stacking sequences of the X-Ga-Ga-X slabs along the *c* direction: GaS prefers the β structure (space group no. 194, $P6_3/mmc$, D_{6h}) while the most common polytype

for GaSe is the ε structure (space group no. 187, P-6m2, D_{3h}). Figure 1a and 1b indicate the layered GaS and GaSe structures. After structural relaxation, the lattice constant for GaS is a=3.573 Å, c=15.511 Å, and for GaSe is a=3.752 Å, c=15.95 Å. In relaxed GaS bulk structure, bond lengths of S-Ga and Ga-Ga are 2.327 Å and 2.451 Å, respectively, while the interlayer distance (S-Ga) is 4.228 Å. In regard to bulk GaSe, the Se-Ga bond length is 2.475 Å, the Ga-Ga bond length is 2.393 Å and the interlayer distance (Se-Ga) is 4.386 Å. As shown in Figure 1c, the band structure of GaS indicates an indirect gap (Γ-M) of 1.6 eV and a direct gap (Γ-Γ) of 1.794 eV. In case of GaSe in bulk phase, the direct band gap (Γ-Γ) of 1.047 eV is identified, as shown in Figure 1d.

The two-dimensional GaS or GaSe monolayer structures are shown in Figure 2a and 2b. In our calculations, the lattice constants for single-layer GaS and GaSe are larger in comparison to the bulk counterparts due to the absence of interlayer interaction. In case of GaS single layer, the lattice constant is a=3.635 Å, while 3.815 Å for GaSe single layer. The bond lengths of S-Ga and Ga-Ga in single-layer GaS are 2.368 Å and 2.479 Å, respectively; while the bond lengths of Se-Ga and Ga-Ga in single-layer GaSe are 2.5 Å and 2.474 Å, respectively. As can be seen from Figure 2c and 2d, the band structures of both single-layer GaS and GaSe demonstrate indirect band gaps and similar band dispersion relation. In comparison to the band structures of corresponding bulk phases, one of the apparent changes in the band structures of single-layer GaS and GaSe is that the valence band maximum (VBM) shifts to two symmetric points near Γ-point in the two-dimensional hexagonal Brillouin zone. In both cases of single-layer GaS and GaSe, the conduction band minimum (CBM) locates at Γ-point. At PBE level

of theory, band gaps of single-layer GaS and GaSe are 2.4 eV and 1.83 eV, respectively, which is in agreement with previous theoretical results.[13,28-30] In the case of single-layer GaS, our results indicate that the energy difference between CBM at Γ- and M-point is small (100 meV), while it is significant for the GaSe single layer (340 meV). As can be seen, the difference between direct and indirect band gaps is small that electrons could transfer easily between the minimum with low thermal energy. However, the band gap nature from previous results is controversial. In Refs. 13, 28, and 29, taking single-layer GaS as an example, the CBM is determined to M-point, whereas at Γ-point in Ref. 30.

In order to explain the conflict of the band gap nature, namely, the position of CBM, we checked the dependence of band structures of single-layer GaS and GaSe on the lattice constants. In comparison to previous works,[13,28-30] we used improved cutoff energy (470 eV), ***k***-point grid (23×23) and vacuum space (30 Å) in the present work to obtain the more accurate lattice constants for single-layer GaS and GaSe. In light of the calculated lattice constants (see above), we address that the CBM for single-layer GaS is located at the Γ-point, which is in agreement with the result in Ref. 30. However, the CBM at Γ-point will shift downward when the lattice constant increases, as shown in Figure 2e of the band structure of single-layer GaS with the lattice constant increased by 0.05 Å. In this case, the CBM energy difference between Γ- and M-point increases, giving rise to an indirect band gap of 2.15 eV. The CBM at Γ-point will shift downward further when the lattice constant increases further. On the other hand, the CBM of single-layer GaS shifts to the M-point when the lattice constant decreases because the CBM at Γ-point rises, which can be attributed to the enhanced interaction between S

and Ga. As illustrated in Figure 2f, even a slight decrease of 0.05 Å of the lattice constant of single-layer GaS will result in the change of CBM position, leading to an indirect band gap of 2.58 eV. In addition, we confirm that the CBM of single-layer GaS at Γ-point will further rise in energy when the lattice constant further decreases. As a consequence, the conflict of the band gap nature of single-layer GaS in previous works can probably be ascribed to the different lattice constant. As an example, the obtained lattice constant of single-layer GaS is 3.58 Å in Ref. 13 and the CBM is determined to M-point; while the CBM is demonstrated to locate at Γ-point based on a lattice constant of 3.63 Å in Ref. 30. A similar behavior is also verified for single-layer GaSe. As a result, it should be pointed out that the band structures of single-layer GaS and GaSe strongly depend on the lattice constant due to the strong *sp* orbital hybridization in GaS and GaSe.[28] In addition, the sensitivity of CBM at Γ-point to vertical electric field has also been found in GaS.[29]

In the presence of weak interlayer interaction, several stacking patterns are allowed in bulk GaS and GaSe.[5,6] In this work, following the stacking patterns in bulk GaS and GaSe above mentioned, two types of GaS/GaSe heterostructures are taken into account. In respect to the first one, single-layer GaS and GaSe slabs are stacked along the [001] direction as the sequence in *β*-GaS bulk structure (see Figure 1a) to form the GaS/GaSe heterobilayer, as indicated in Figure 3a and 3c. In this case, the in-plane lattice constant of the GaS/GaSe heterostructure is set as the lattice constant of single-layer GaS, and such a type of GaS/GaSe heterostructure is referred to as *β*-type. It corresponds to the epitaxial growth of GaSe on GaS substrate in experiment. It should be pointed out that

the lattice mismatch (4.72%) between single-layer GaS and GaSe can introduce strain to the heterointerfaces. In respect to the second one, single-layer GaS and GaSe slabs are stacked as the sequence in layered ε-GaSe in c direction and the lattice constant of single-layer GaSe is used as the in-plane lattice constant of GaS/GaSe heterobilayer. It corresponds to the epitaxial growth of GaS on GaSe substrate in experiment. As shown in Figure 3b and 3d, such a type of GaS/GaSe heterostructure is referred to as ε-type. In β-type GaS/GaSe heterobilayer, top-layer Ga (Se) atoms are superimposed on the bottom-layer S (Ga) atoms. In ε-type GaS/GaSe heterobilayer, Se atoms of the top layer are superimposed on Ga atoms of the bottom layer, and the top-layer Ga atoms are above the hexagon centers formed by bottom-layer S atoms. It should be pointed out that the relative orientation angle between GaS and GaSe could probably change the electronic properties.[31] After full relaxation, structural information for both β- and ε-type GaS/GaSe heterostructures are summarized in Table 1. In comparison to single-layer GaS and GaSe, S-Ga bond length obviously increases, while Se-Ga bond length is almost unchanged. In both types of the GaS/GaSe heterostructures, interlayer distances increases compared to GaS and GaSe in bulk phases, indicating the decreased interlayer interaction. In the energy-minimum situation, the interlayer distances are 4.8 Å and 4.861 Å for β- and ε-type GaS/GaSe heterostructures, respectively. In order to check the stability of the heterostructures of GaS/GaSe, we calculated the binding energy as follows

$$E_B = E_{GaS/GaSe} - E_{GaS} - E_{GaSe}$$

where $E_{GaS/GaSe}$, E_{GaS} and E_{GaSe} represent the total energies of GaS/GaSe heterostructure,

single-layer GaS and single-layer GaSe, respectively. According to the equation defined above, the binding energies for β- and ε-type GaS/GaSe heterostructures are -0.132 eV and -0.314 eV, respectively. In respect to MoS_2/$MoSe_2$ heterobilayers, which have been reported experimentally,[32] the binding energies are in a range of -0.1 eV~-0.2 eV.[33] In addition, the binding energy for graphene/MoS_2 heterobilayer is -0.023 eV per carbon atom.[34] As a result, the more negative binding energy compared to MoS_2/$MoSe_2$ or graphene/MoS_2 heterostructures is an indication that the interfaces between single-layer GaS and GaSe are energetically stable and easy to realize in experiments.

It has been demonstrated experimentally that interlayer interactions between single-layer MoS_2 and WS_2 could be tuned from noncoupling to strong coupling and thus the properties should be affected.[18] Analogously, we studied the relation between interlayer interaction and electronic structures in heterostructures of GaS/GaSe. In this work, the interlayer distance is randomly increased or decreased by a small step to get the general trend, rather than a constant interval. As the interlayer distance increases, with the interlayer interaction decreasing, band gaps of both β- and ε-type GaS/GaSe heterostructures decrease. As indicated in Figure 4a and 4d, band gaps varies in a small range, namely, 0.85-0.89 eV for β-type GaS/GaSe heterostructure and 1.13-1.27 eV for the ε-type. It is apparent that the band gap of heterostructures is rather weakly sensitive to the interlayer distance. In comparison to single-layer GaS (2.4 eV) and GaSe (1.83 eV), however, band gaps of GaS/GaSe heterostructures are substantially reduced. In previous theoretical work, band offset between single-layer GaS and GaSe was demonstrated to be a type-II alignment,[13] which can be further confirmed by the band

gap reduction. In accordance with the VBM and CBM energy levels with respect to the redox potentials of water splitting, single-layer GaS and GaSe were suggested to be suitable photocatalysts.[13] In applications in photocatalyst, type-II alignment formed in GaS/GaSe heterostructures is an indication of reduced carrier recombination and thus the improved energy conversion efficiency. However, S- and Se-based compounds are not good candidates for photocatalysts because of environmental problem. In addition to the reduced band gaps, appropriate positions of electronic band edges of GaS/GaSe heterostructures are another important metric for determining the capability to function in a solar energy conversion process.[35]

In order to get an intuitional insight, the band structures of the two types of GaS/GaSe heterostructures are shown in Figure 5, which indicates that the band gaps of β-type and ε-type GaS/GaSe heterostructures are 0.87 eV and 1.2 eV, respectively. On the basis of the orbital character, the conduction and valence bands are shown in different colors ranging from blue (contributions from GaSe) to red (contributions from GaS). As can be noticed, the CBM is mainly contributed from GaS while the VBM is predominately ascribed to GaSe, revealing the formation of type-II band alignment. It is an indication that the photoexcited electrons and holes would distribute on opposite constituents of the heterostructure, enabling the efficient separation. In applications in optoelectronics and solar energy conversion, physical separation of photoexcited carriers plays a vital role in the high performance due to the significant reduction of carrier recombination. In low-dimensional materials, excitonic effects dominate the optical properties with the formation of bound excitons of large binding energy.[36,37] In single-layer GaS or GaSe,

the strong interaction between photoexcited electrons and holes enhances the possibility of recombination. In the GaS/GaSe heterostructures, such Coulomb interactions should be weakened due to the enhanced screening effects. As a result, constituent single-layer GaS and GaSe would act as charge separators, resulting in the enhancement of exciton dissociation. In this respect, GaS/GaSe heterostructures manifest superiority to single-layer GaS and GaSe when they are used as photodetector and photocatalysis. In regard to other GaS/GaSe heterostructures with various interlayer distances, similar electronic band structures can be verified.

It often requires tunable electronic properties that can be deliberately modulated by external parameters in applications of two-dimensional materials as controllable and tunable electronic devices. Hereinto, applying strain is always a powerful approach to tune the electronic and optical features of two-dimensional materials. It has been shown that the elastic moduli of GaS and GaSe are rather smaller than that of MoS_2, suggesting that single-layer GaS and GaSe are softer than MoS_2 and thus can be easily strained.[13] As a consequence, how the electronic structures of GaS/GaSe heterostructures will be affected by strain is examined in this work.

As demonstrated in Figure 4b and 4e, biaxial tensile strain can approximately linearly reduce the band gap of GaS/GaSe heterostructures. In case of applying strain of 2% for β-type and ε-type heterostructures, band gaps can be substantially reduced by 0.23 eV and 0.24 eV, respectively. As the biaxial strain increases to 10%, band gap of the β-type heterostructure is 0.12 eV and 0.38 eV for the ε-type. In respect to the band structures, we confirm that the CBM maintains at Γ-point and continuously shifts downward when

the strain is increased. As a representative, band structures along K-Γ-M for GaS/GaSe heterostructures under strain of 10% are shown in Figure 6a and 6c, from which we can see that the band dispersion relation in valence bands is slightly changed compared to that of single-layer GaS and GaSe.

The energy difference between strained and unstrained heterostructures reflects the influence of strain on the structural and elastic properties, which can be illustrated as[30]

$$E_S = E_T(s) - E_T(s=0)$$

where $E_T(s)$ and $E_T(s=0)$ are the total energies of GaS/GaSe heterostructures under a given strain s and without strain, respectively. As demonstrated in Figure 4c and 4f, for both types of GaS/GaSe heterostructures, the strain energy increases monotonically as the strain varies from 2% to 10%. Under a strain of 10%, the strain energy is as large as 1.72 eV for the β-type GaS/GaSe heterostructure while 2.21 eV for the ε-type, which are significantly higher than those for single-layer GaS and GaSe.[30] In cases of single-layer GaS and GaSe, biaxial tensile strain can also obviously reduce the band gap.[13,28,30] In practical applications, tunable band gap means spectrum selectivity.

In addition, the van der Waals heterostructures of GaS/GaSe with structural inversion asymmetry lead to nontrivial phenomenon, such as the Rashba spin splitting. As shown in Figures 6b and 6d, in consideration of SOC effects, significant Rashba spin splitting occurs in GaS/GaSe heterostructures (under biaxial strain of 10%, and the Rashba spin splitting also occurs in the other cases with strain of 0-8%). However, the band gaps are almost unchanged compared with those calculated without considering the SOC effects, which can be attributed to the absence of heavy elements in GaS/GaSe heterostructures.

As can be seen, particularly, the Rashba effects occur not only to electrons in conduction bands but also to holes in valence bands. In consideration of the type-II band alignment, the Rashba spin splitting in GaS/GaSe heterostructures occurs independently in the two constituents. In previous reports, the Rashba effects are verified in AlGaAs/GaAs and InAs/GaSb quantum wells, heavy metal surfaces Au(111) and Bi(111), and hypothetical two-dimensional structures such as $LaOBiS_2$, $SrFBiS_2$, $BiOBiS_2$, BiTeBr and BiTeI.[38-45] It is apparent that the exciting superiority of GaS/GaSe heterostructures as a Rashba system lies in the absence of heavy metal atoms. Here, we notice that two-dimensional van der Waals heterostructures with Rashba spin splitting have never been reported before.

Figures 7a and 7b show the spin textures of the VBM and CBM of β-type GaS/GaSe heterostructure under a biaxial strain of 10%, confirming the occurrence of the Rashba effects. As shown in the spin textures, we can see the helical Rashba spin polarizations perpendicular to the momentums. In particular, spin orientations in VBM are opposite to those in CBM. As Figure 7c demonstrated, holes in the VBM of ε-type GaS/GaSe heterostructure exhibit some spin polarizations parallel to the momentums, which can be considered as the Rashba-Dresselhaus spin splitting. In case of the CBM of ε-type GaS/GaSe heterostructure, spin textures shown in Figure 7d confirm the Rashba spin splitting. As consequence, realization of the Rashba effects makes the two-dimensional GaS/GaSe heterostructures to be promising candidates in ultrathin spintronic devices.

4. Conclusion

Vertically stacked GaS and GaSe single layers demonstrate a new member of van der Waals heterostructures with tunable physical and optical properties. It holds the great promise for a wide range of applications in such as electronics, optoelectronics as well as spintronics, suggesting a potential to realize the truly two-dimensional nanodevices. In this work, we found that the GaS/GaSe heterostructures could play a role as exciton separators to physically separate the electrons and holes, which marks the possibility of substantially improved energy conversion efficiency. In particular, the Rashba effects were firstly found in the two-dimensional GaS/GaSe heterostructures. In addition, we also confirmed that the electronic properties of GaS/GaSe heterostructures can be tuned by strain, which is highly desirable in electronic devices.

Acknowledgements

The authors acknowledges financial support from the National Basic Research Program of China (973 program, 2013CB632401), the National Science Foundation of China under grant 11374190, 21333006 and 11404187; and the Fundamental Research Funds of Shandong University is also acknowledged.

References

1 Th. Köhler, Th. Frauenheim, Z. Hajnal and G. Seifert, *Phys. Rev. B* 2004, **69**, 193403.

2 U. K. Gautam, S. R. C. Vivekchand, A. Govindaraj, G. U. Kulkarni, N. R. Selvi and C. N. R. Rao, *J. Am. Chem. Soc.* 2005, **22**, 3658.

3 D. Errandonea, A. Segura, F. J. Manjón, A. Chevy, E. Machado, G. Tobias, P. Ordejón, and E. Canadell, *Phys. Rev. B* 2005, **71**, 125206.

4 D. V. Rybkovskiy, A. V. Osadchy and E. D. Obraztsova, *Phys. Rev. B* 2014, **90**, 235302.

5 Z. Zhu, Y. Cheng and U. Schwingenschlögl, *Phys. Rev. Lett.* 2012, **108**, 266805.

6 W. An, F. Wu, H. Jiang, G.-S. Tian, and X.-Z. Li, *J. Chem. Phys*. 2014, **141**, 084701.

7 D. J. Late, B. Liu, H. S. S. R. Matte, C. N. R. Rao and V. P. Dravid, *Adv. Funct. Mater.* 2012, **22**, 1894.

8 D. J. Late, B. Liu, J. Luo, A. Yan, H. S. S. R. Matte, M. Grayson, C. N. R. Rao and V. P. Dravid, *Adv. Mater.* 2012, **24**, 3549.

9 P. Hu, Z. Wen, L. Wang, P. Tan and K.; Xiao, *ACS Nano* 2012, **7**, 5988.

10 P. Hu, L. Wang, M. Yoon, J. Zhang, W. Feng, X. Wang, Z. Wen, J. C. Idrobo, Y. Miyamoto, D. B. Geohegan, and K. Xiao, *Nano Lett.* 2013, **13**, 1649.

11 S. Lei, L. Ge, Z. Liu, S. Najmaei, G. Shi, G. You, J. Lou, R. Vajtai and P. M. Ajayan, *Nano Lett.* 2013, **13**, 2777.

12 Y. Zhou, Y. Nie, Y. Liu, K. Yan, J. Hong, C. Jin, Y. Zhou, J. Yin, Z. Liu and H. Peng, *ACS Nano* 2014, **2**, 1485.

13 H. L. Zhuang, and R. G. Hennig, *Chem. Mater.* 2013, **25**, 3232.

14 L. A. Ponomarenko, R. V. Gorbachev, G. L. Yu, D. C. Elias, R. Jalil, A. A. Patel, A. Mishchenko, A. S. Mayorov, C. R. Woods, J. R. Wallbank, M. Mucha-Kruczynski, B. A. Piot, M. Potemski, I. V. Grigorieva, K. S. Novoselov, F. Guinea, V. I. Fal'ko and A. K. Geim, *Nature* 2013, **497**, 594.

15 C. R. Dean, L. Wang, P. Maher, C. Forsythe, F. Ghahari, Y. Gao, J. Katoch, M. Ishigami, P. Moon, M. Koshino, T. Taniguchi, K. Watanabe, K. L. Shepard, J. Hone and P. Kim, *Nature* 2013, **497**, 598.

16 Y. Gong, J. Lin, X. Wang, G. Shi, S. Lei, Z. Lin, X. Zou, G. Ye, R. Vajtai, B. I. Yakobson, H. Terrones, M. Terrones, B. K. Tay, J. Lou, S. T. Pantelides, Z. Liu, W. Zhou and P. M. Ajayan, *Nature Mater.* 2014, **13**, 1135.

17 L. Kou, T. Frauenheim, and C. Chen, *J. Phys. Chem. Lett.* 2013, **4**, 1730.

18 S. Tongay, W. Fan, J. Kang, J. Park, U. Koldemir, J. Suh, D. S. Narang, K. Liu, J. Ji and J. Li, *Nano Lett.* 2014, **14**, 3185.

19 N. Myoung, K. Seo, S. J. Lee and G. Ihm, *ACS Nano* 2013, **7**, 7021.

20 M. Bernardi, M. Palummo and J. C. Grossman, *Nano Lett.* 2013, **13**, 3664.

21 G. Kresse, and J. Furthmuller, *Phys. Rev. B* 1996, **54**, 11169.

22 G. Kresse, and J. Joubert, *Phys. Rev. B* 1999, **59**, 1758.

23 J. P. Perdew, and Y. Wang, *Phys. Rev. B* 1992, **45**, 13244.

24 J. P. Perdew, K. Burke and M. Ernzerhof, *Phys. Rev. Lett.* 1996, **77**, 3865.

25 H. J. Monkhorst and J. D. Pack, *Phys. Rev. B* 1976, **13**, 5188.

26 S. Grimme, *J. Comput. Chem.* 2006, **27**, 1787.

27 A. D. Corso, and A. M. Conte, *Phys. Rev. B* 2005, **71**, 115106.

28 Y. Ma, Y. Dai, M. Guo, L. Yu and B. Huang, *Phys. Chem. Chem. Phys.* 2013, **15**, 7098.

29 Y. Li, H. Chen, L. Huang and J. Li, *J. Phys. Chem. Lett.* 2015, **6**, 1059.

30 L. Huang, Z. Chen and J. Li, *RSC Adv.* 2015, **5**, 5788.

31 O. Neufeld and M. C. Toroker, *Phys. Chem. Chem. Phys.* 2015, **17**, 24129.

32 F. Ceballos, M. Z. Bellus, H.-Y. Chiu and H. Zhao, *ACS Nano* 2014, **8**, 12717.

33 J. Kang, J. Li, S.-S. Li, J.-B. Xia and L.-W. Wang, *Nano Letter* 2013, **13**, 5485.

34 Y. Ma, Y. Dai, M. Guo, C. Niu and B. Huang, *Nanoscale* 2011, **3**, 3883.

35 M. C. Toroker, D. K. Kanan, N. Alidoust, L. Y. Isseroff, P. Liaob and E. A. Carter, *Phys. Chem. Chem. Phys.* 2011, **13**, 16644.

36 W. Wei and T. Jacob, *Phys. Rev. B* 2013, **87**, 115431.

37 W. Wei and T. Jacob, *Phys. Rev. B* 2013, **87**, 085202.

38 G. Lommer, F. Malcher and U. Rossler, *Phys. Rev. Lett.* 1988**, 60**, 728.

39 J. Nitta, T. Akazaki, H. Takayanagi and T. Enoki, *Phys. Rev. Lett.* 1997**, 78**, 1335.

40 S. LaShell, B. A. McDougall and E. Jensen, *Phys. Rev. Lett.* 1996, **77**, 3419.

41 Y. M. Koroteev, G. Bihlmayer, J. E. Gayone, E. V. Chulkov, S. Blugel, P. M. Echenique and P. Hofmann, *Phys. Rev. Lett.* 2004, **93**, 046403.

42 A. Kimura, E. E. Krasovskii, R. Nishimura, K. Miyamoto, T. Kadono, K. Kanomaru, E. V. Chulkov, G. Bihlmayer, K. Shimada, H. Namatame and M. Taniguchi, *Phys. Rev. Lett.* 2010, **105**, 076804.

43 Y. Ma, Y. Dai, N. Yin, T. Jing and B. Huang, *J. Mater. Chem. C* 2014, **2**, 8539.

44 Y. Ma, Y. Dai, W. Wei, X. Li and B. Huang, *Phys. Chem. Chem. Phys.* 2014, **16**, 17603.

45 Q. Liu, Y. Guo and A. J. Freeman, *Nano Lett.* 2013, **13**, 5264.

Table 1 Structural information for ralaxed β-type and ε-type GaS/GaSe heterostructures: S-Ga bond length ($l_{S\text{-}Ga}$), Se-Ga bond length, Ga-Ga bond length in GaS ($l_{Ga\text{-}Ga\text{-}1}$) layer, Ga-Ga bond length in GaSe ($l_{Ga\text{-}Ga\text{-}2}$) layer and interlayer distance (d). The unit is in Å.

types	$l_{S\text{-}Ga}$	$l_{Se\text{-}Ga}$	$l_{Ga\text{-}Ga\text{-}1}$	$l_{Ga\text{-}Ga\text{-}2}$	d
β	2.425	2.501	2.491	2.482	4.8
ε	2.421	2.499	2.481	2.47	4.861

Figure Captions

Figure 1. Side view of (a) GaS and (b) GaSe structures in bulk phase, the big (purple) and small (green and dark yellow) spheres represent Ga and S (Se) atoms, respectively. Band structures of (c) GaS and (d) GaSe in bulk phase, the red dashed lines indicate the Fermi levels, which are set to zero.

Figure 2. (a) Top and (b) side views of single-layer GaS (GaSe), the big (purple) and small (green) spheres represent Ga and S (Se) atoms, respectively; a rhombus represents a unit cell. Band structures of (c) single-layer GaS, (d) single-layer GaSe, (e) single-layer GaS with lattice constant increased by 0.05 Å, and (f) single-layer GaS with lattice constant decreased by 0.05 Å. The dashed lines indicate the Fermi levels, which are set to zero.

Figure 3. (a) Top and (c) side views of β-type GaS/GaSe heterostructures, (b) top and (d) side views of ε-type GaS/GaSe heterostructures. The big (purple) and small (green) spheres represent Ga and S (Se) atoms, respectively. The arrows indicate the interlayer distance d.

Figure 4. Band gap evaluation of β-type GaS/GaSe heterostructure as a function of (a) interlayer distance and (b) strain; band gap evaluation of ε-type GaS/GaSe heterostructure as a function of (d) interlayer distance and (e) strain. Strain energy of (c) β-type and (f) ε-type GaS/GaSe heterostructure as a function of strain.

Figure 5. Band structures of (a) β-type and (b) ε-type GaS/GaSe heterostructures on the basis of the orbital character, where the conduction and valence bands are demonstrated in different colors ranging from blue (contributions from GaSe) to red (contributions from GaS). The dashed lines indicate the Fermi levels, which are set to zero.

Figure 6. Band structures of β-type GaS/GaSe heterostructure under a biaxial strain of 10% (a) without and (b) with the consideration of SOC effects; and of ε-type GaS/GaSe heterostructure under a biaxial strain of 10% (c) without and (d) with the consideration of SOC effects. The dashed lines indicate the Fermi levels, which are set to zero.

Figure 7. Spin textures for (a) VBM and (c) CBM of β-type GaS/GaSe heterostructure; (c) VBM and (d) CBM of ε-type GaS/GaSe heterostructure. The arrows indicate the in-plane orientation of spin, and color background denotes the z component of spin.

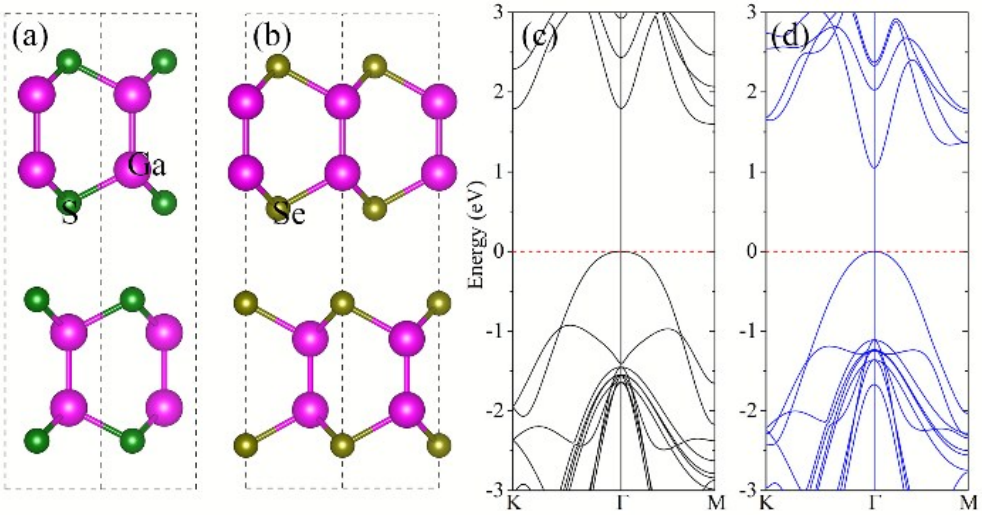

Figure 1

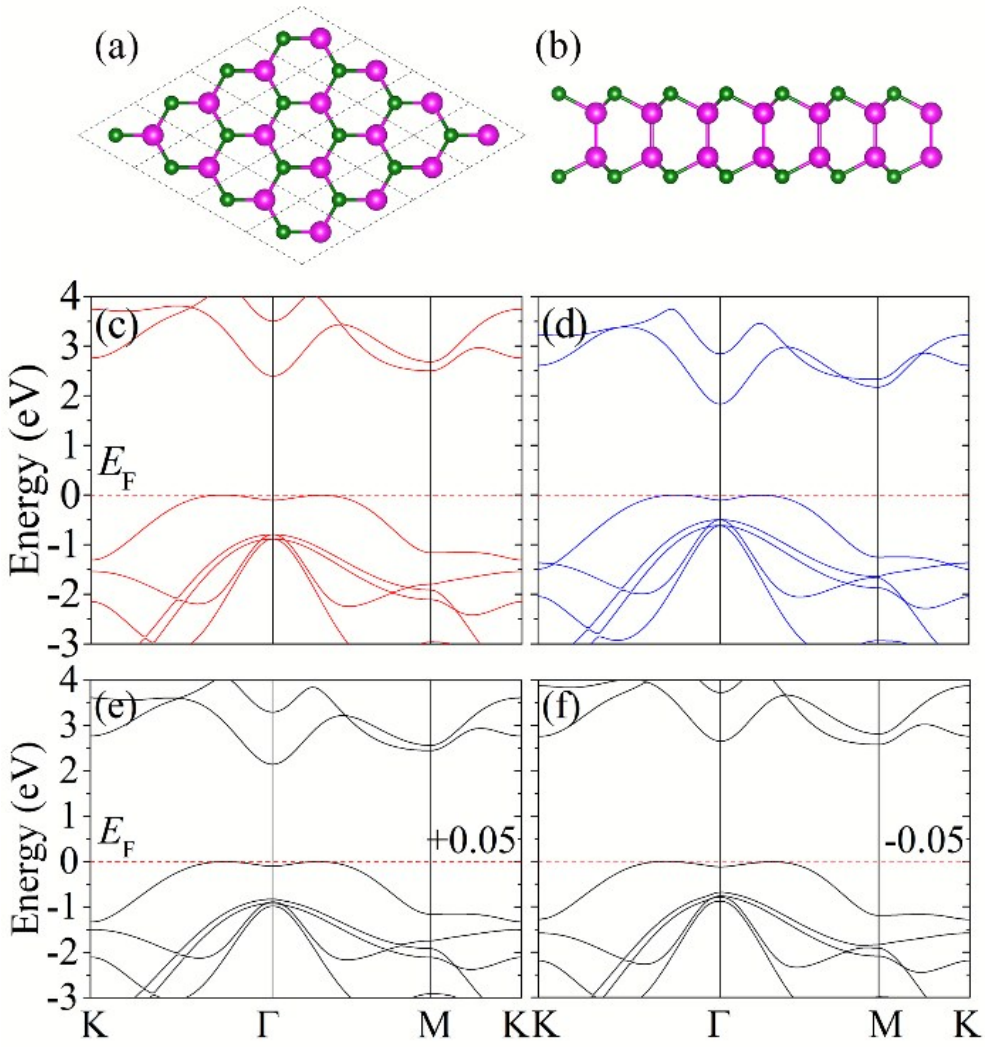

Figure 2

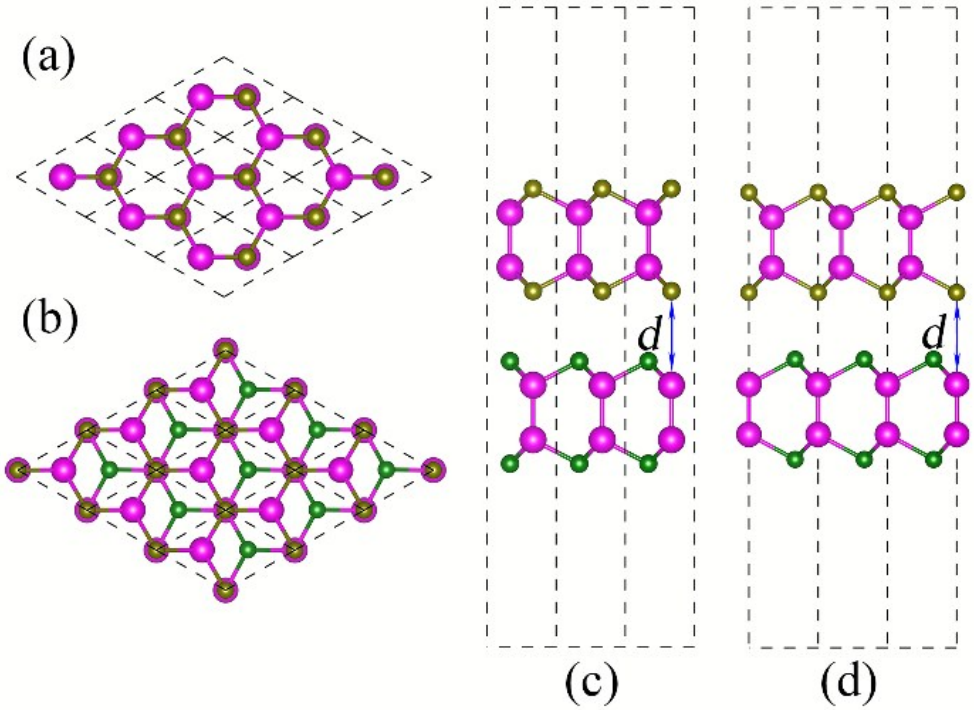

Figure 3

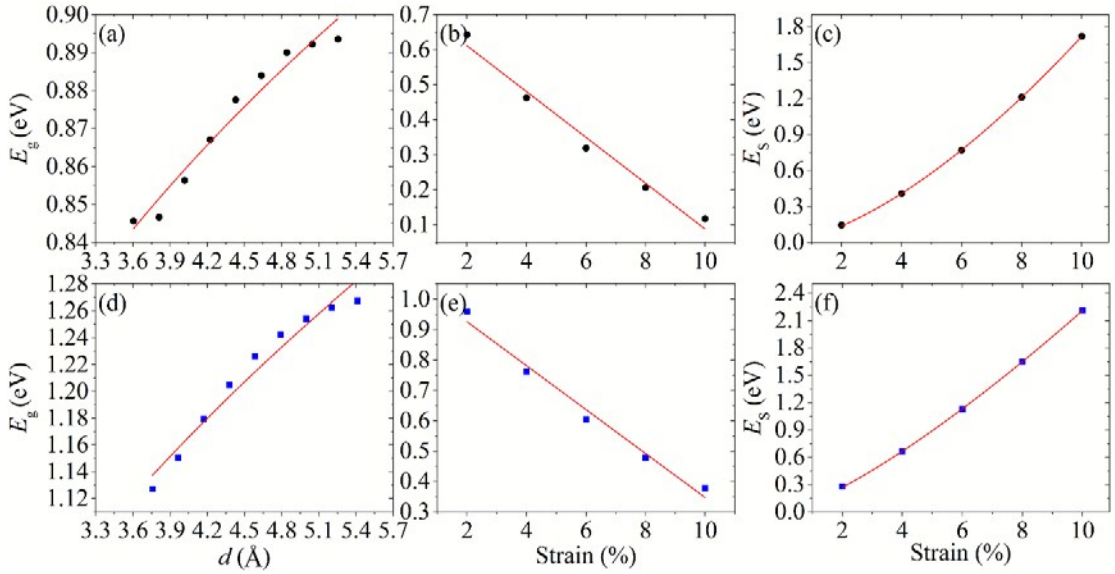

Figure 4

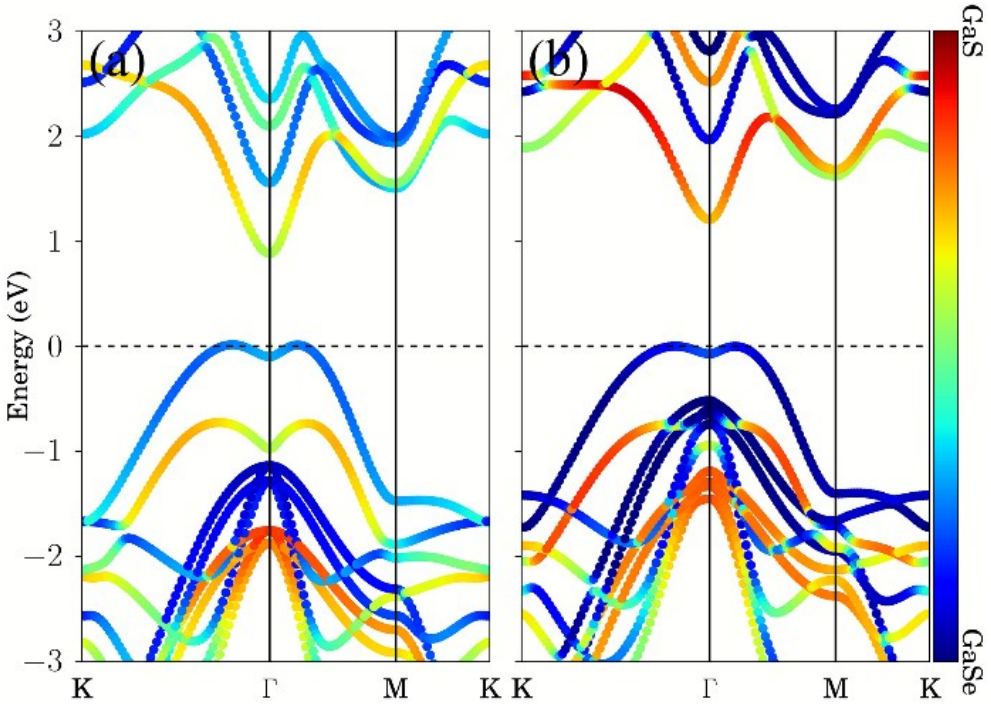

Figure 5

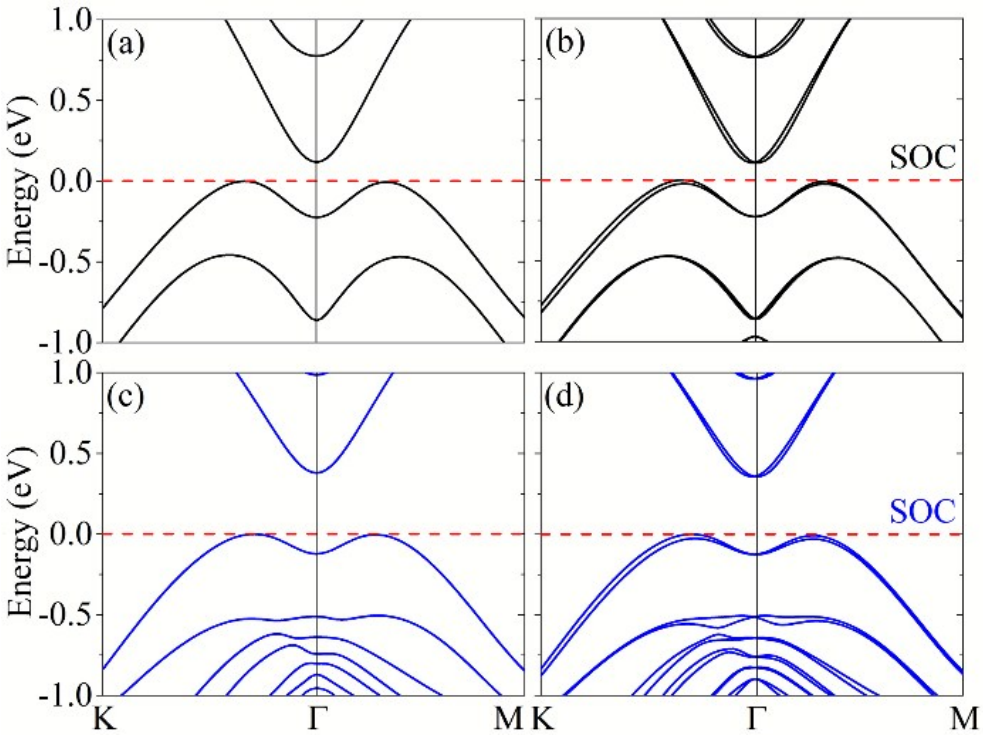

Figure 6

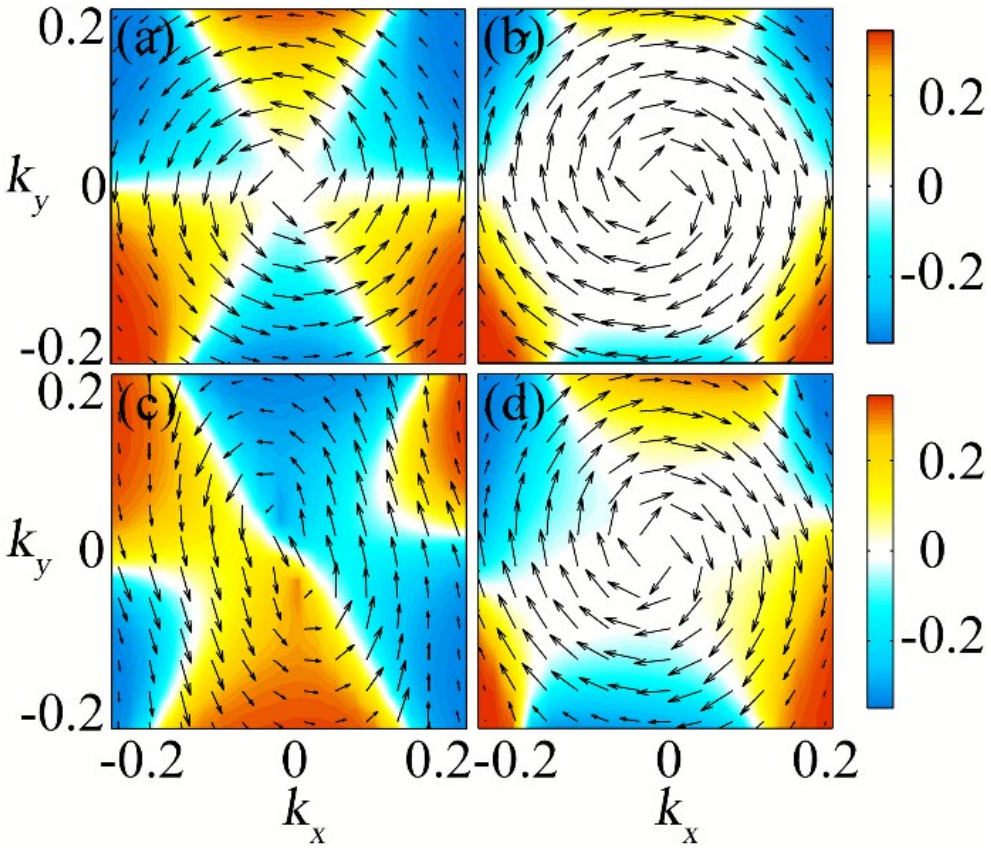

Figure 7